International Journal of Heat and Mass Transfer 79 (2014) 291–299

Contents lists available at ScienceDirect

International Journal of Heat and Mass Transfer

journal homepage: www.elsevier.com/locate/ijhmt

Constructal design of thermoelectric power packages

Adrian Bejan [a,*], Sylvie Lorente [b], Deok-Hong Kang [c]

[a] Department of Mechanical Engineering and Materials Science, Duke University, Durham, NC 27708-0300, USA
[b] Université de Toulouse, INSA, 135 Avenue de Rangueil, 31077 Toulouse, France
[c] Research Institute of Industrial Science and Technology, Energy & Resources Research Department, Pohang, Republic of Korea

ARTICLE INFO

Article history:
Received 11 July 2014
Received in revised form 4 August 2014
Accepted 5 August 2014
Available online 28 August 2014

Keywords:
Thermoelectric
Constructal
Vascular
Serpentine

ABSTRACT

In this paper we consider the complete thermofluid design and performance of a thermoelectric module. We increase the temperature difference that must be maintained across the module, and at the same time we reduce the pumping power required by the streams that bathe the hot and cold plates of the module. We find that for greater power output the two streams must be configured in parallel, not in counterflow, and not between two well mixed plenums. We also find that the loss of thermoelectric power due to the temperature nonuniformity of the two plates competes with the power lost during the pumping of the two streams, and that from this competition results the optimal mass flow rates of the two streams. At the optimum, the maximized power output of the module is proportional to a group of geometric parameters (Eq. (39)), which can be maximized further by designing vascular flow architectures for the two plates. The vascular designs reveal an optimal ratio of channel diameters, optimal plate aspect ratio, and a channel flow volume fraction that is of the same order as the ratio of the fluid thermal conductivity divided by the solid thermal conductivity. The flow architectures are further illustrated with numerical examples of vascular and serpentine configuration and performance.

1. Thermoelectric power generation

Thermoelectric power generation (TE) is attracting interest from across the spectrum of technology because it offers a path to clean, renewable energy. In addition, TE devices offer compactness and simplicity because they do not have moving parts. The efficiency of TE designs is limited by the transport properties of the thermoelectric materials accounted for in the property group Z discussed in Eq. (1). Progress toward greater efficiencies can be made by optimizing the geometry—the relative shapes and sizes—of the legs of the module [1–3]. This and other aspects of the optimization of thermoelectric modules (TEM) has generated a growing body of literature [1–19].

In the present study we consider the whole picture—the thermofluid design and performance of the TEM. We consider not only the temperature difference that must be maintained across the TEM, but also the fluid mechanics of the vascular hot and cold plates that sandwich the TEM. We show that important tradeoffs exist in the thermofluid design such that the overall performance of the TEM is increased.

The thermoelectric module (TEM) is defined in Fig. 1. The hot plate is heated by a stream of hot oil. The cold plate is cooled by a stream of water. Heat flows by conduction perpendicular to the plates, from the hot plate to the cold plate.

Larger stacks are obtained by sandwiching several TEMs as shown in Fig. 2. All the TEMs are identical. Each is a sandwich of three parts: hot plate (H), thermoelectric converter (T), and cold plate (C), in other words, HTC, or CTH. There are two ways to assemble such elements in a stack:

(a) Alternating orientations, i.e., plates of the same temperature touching each other:

HTC CTH HTC...

(b) Elements oriented in the same way:

HTC I HTC I HTC...

The simplest design is (a). In design (b), a layer of insulation (I) must be placed between the C and H plates of adjacent elements. Fig. 2 shows the (a) rule of assembly.

If the TEM is small enough and the hot and cold fluid flow rates are large enough, then the hot and cold plates are essentially isothermal, at T_H and T_L, respectively. The thermodynamics of the TEM is detailed in Ref. [1], and it shows that the maximum thermodynamic efficiency of a module with isothermal ends is

* Corresponding author.
E-mail address: abejan@duke.edu (A. Bejan).

http://dx.doi.org/10.1016/j.ijheatmasstransfer.2014.08.008
0017-9310/

Nomenclature

A	plate area, m^2
C	factor, dimensionless
c_P	specific heat at constant pressure, J kg^{-1} K^{-1}
d	spacing between channels, m
D_2	channel thickness scale, m
D_1	trunk thickness, m
D_2	branch thickness, m
G	function of geometry, Eq. (39)
H	transversal dimension of area, m
I	integral
k	effective TEM thermal conductivity, W m^{-1} K^{-1}
k_f	fluid thermal conductivity, W m^{-1} K^{-1}
k_s	solid plate conductivity, W m^{-1} K^{-1}
$K_{1,2}$	factors, Eqs. (37) and (38)
L	transverse dimension of area, m
L_s	length scale, m
m	number of channels (branches)
$\dot{m}$	mass flow rate, kg s^{-1}
n	number of channels (branches)
N	number of heat transfer units, Eq. (11)
p	perimeter of contact, m
P	pressure, Pa
q_H	heat current, W
R	electric resistance, Ω
R_{th}	thermal resistance, K W^{-1}
Sv	svelteness number
t	thickness of TEM, m
t	spacing between channels, m
T_H	high temperature, K
T_L	low temperature, K
TEM	thermoelectric module
U	overall heat transfer coefficient, W m^{-2} K^{-1}
V	volume, m^3
W	power, W
W_{lost}	lost power, W
W_{max}	maximum power, W
$W_{\Delta P}$	pumping power, W
$W_{\Delta T}$	power lost due to temperature nonuniformity, W
x	longitudinal coordinate, m
Z	group of properties, Eq. (1)
$\tilde{Z}$	function of Z, Eq. (26)

Greek symbols

δ	spacing between branches, m
ΔP	pressure difference, Pa
ΔT	temperature difference, K
η	efficiency, Eq. (2)
η_p	pump isentropic efficiency
ν	kinematic viscosity, m^2 s^{-1}
ξ	dimensionless longitudinal coordinate
ρ	density, kg m^{-3}
ϕ	area fraction
φ	porosity
ϕ_c	critical area fraction

Subscripts

c	cold
f	fluid
p	plates
counter	counter flow
h	hot
in	inlet
min	minimum
opt	optimum
para	parallel flow

$$\eta_{max} = \frac{T_H - T_L}{T_H} \cdot \frac{Z - 1}{Z + T_L/T_H} \tag{1}$$

where Z (constant) represents a group of thermophysical properties of the material structure sandwiched between T_H and T_L. The energy conversion efficiency is defined as

$$\eta = \frac{I^2 R}{q_H} \tag{2}$$

where I^2R is the delivered electrical power, and q_H is the total heat transfer rate from T_H to T_L. The power I^2R is associated with the flow of the generated current I through an external electrical resistance R.

The heat current q_H is proportional to the temperature difference that drives it,

$$q_H = \frac{T_H - T_L}{R_{th}} \tag{3}$$

where R_{th} is the thermal resistance of the TEM structure held between T_H and T_L. By combining Eqs. (1)–(3) we arrive at the important conclusion that maximum power is delivered in proportion with $(T_H - T_L)^2$,

$$(I^2R)_{max} = (T_H - T_L)^2 \cdot \frac{Z - 1}{R_{th} T_H (Z + T_L/T_H)} \tag{4}$$

The chief conclusion that follows from thermodynamics [1] is that maximum power is achieved in proportion with the temperature difference *squared*. When the volume of the TEM is fixed, maximum power also means maximum power *density*. The route to better designs with greater power density consists of maintaining the largest temperature difference across the TEM, between any point on the hot plate and its projection on the cold plate.

When the hot and cold plates are not isothermal, the design rule identified above becomes critical, and it applies at every point in the plane of the hot plate or the cold plate.

The largest temperature difference available is the difference between the inlet of the hot stream ($T_{h,in}$) and the inlet of the cold stream ($T_{c,in}$). Ideally, the thermo-fluid design of the TEM should be such that the hot plate is isothermal at $T_{h,in}$, and the cold plate is isothermal at $T_{c,in}$. This design would require thick high-conductivity bodies for the hot and cold plates, which increase the weight and decrease the power density of the TEM.

The challenge is to design the TEM when its hot and cold plates are large and not isothermal. This can be achieved by vascularizing the two plates such that, although nonuniform, the *local* temperature difference $(T_h - T_c)$ distribution is such that the integral of $(T_h - T_c)^2$ over the plane of the plate is the largest (Fig. 3).

2. Parallel flow, or counterflow?

Consider first the unidirectional flow configuration shown in Fig. 4. The hot stream flows as a sheet in one direction (x) parallel to the sheet flow of cold fluid. The capacity rates of the two streams are the same, $\dot{m}c_P$. The stream temperatures vary in the longitudinal direction, $T_h(x)$ and $T_c(x)$. When the streams are configured in parallel flow (Fig. 4), the first law of thermodynamics for each stream control volume of length dx requires

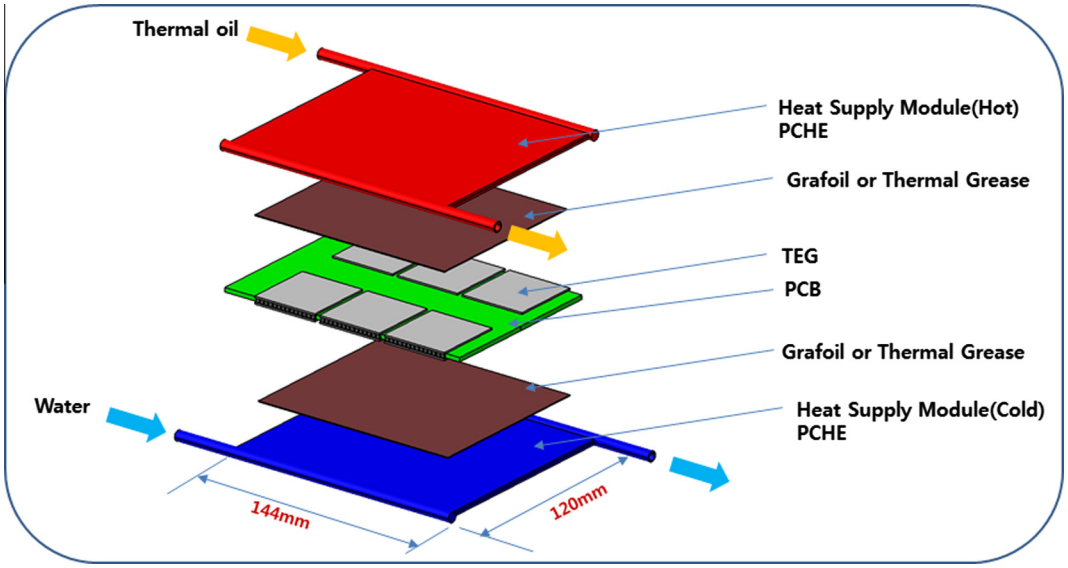

Fig. 1. The main features of the thermoelectric module.

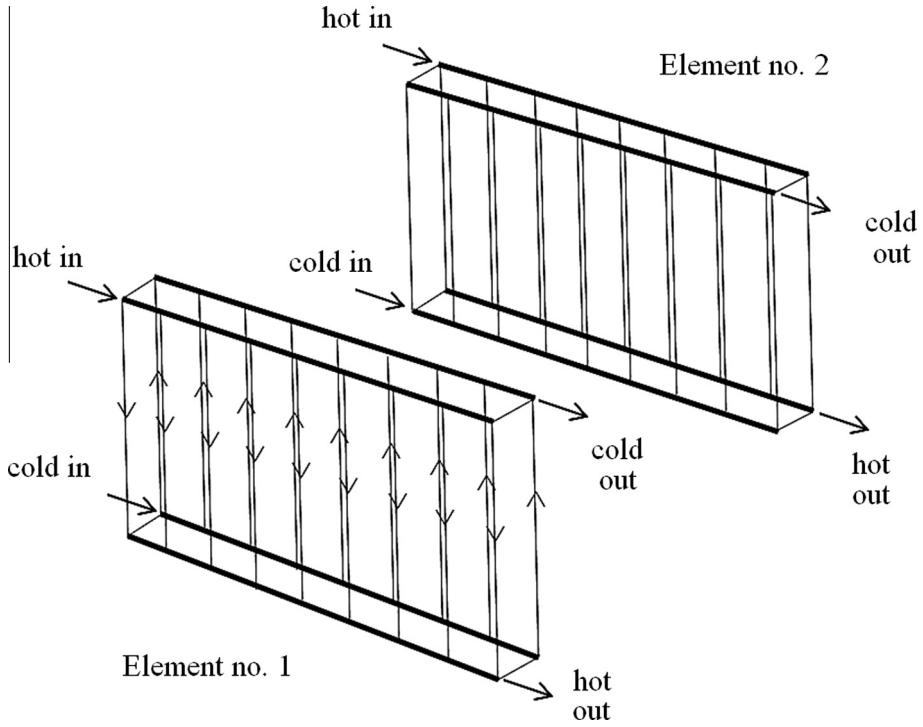

Fig. 2. Stack of two modules, showing the rule of assembly where plates of the same temperature touch each other.

$$-\dot{m}c_P\,dT_h = q'dx \tag{5}$$

$$\dot{m}c_P\,dT_c = q'dx \tag{6}$$

where the stream-to-stream heat transfer rate q' [W/m] is

$$q' = Up(T_h - T_c) \tag{7}$$

where p is the line of thermal contact in the direction perpendicular to Fig. 4, and $U = k/t$ is a constant representing the effective thermal conductivity (k) between the T_h and T_c plates, and the thickness of the structure held between the two plates (t). Combining Eqs. (5)–(7) and integrating from the common inlet ($x = 0$) where $T_h - T_c = T_{h,in} - T_{c,in}$, we obtain the temperature difference distribution

$$\Delta T = \Delta T_{in} e^{-N\xi} \tag{8}$$

$$\text{where } \Delta T = T_h(x) - T_c(x) \tag{9}$$

$$\Delta T_{in} = T_{h,in} - T_{c,in} \tag{10}$$

$$N = \frac{UpL}{\dot{m}c_P} \tag{11}$$

$$\xi = \frac{x}{L} \tag{12}$$

and $pL = A$ is the area of the plate, in other words, $N = (k/t)A/(\dot{m}c_P)$. According to Eq. (4), the power density of the parallel flow design is proportional to the integral

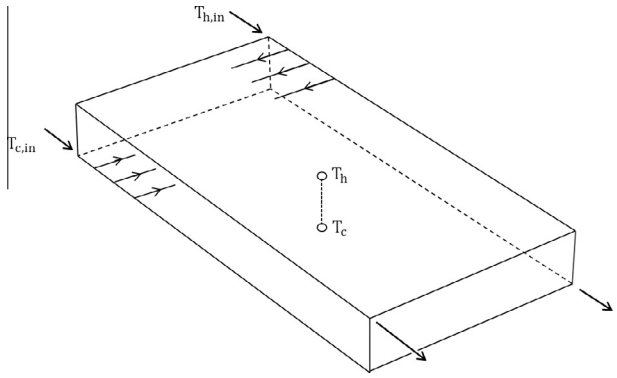

Fig. 3. The local temperature difference $T_h - T_c$ across a module.

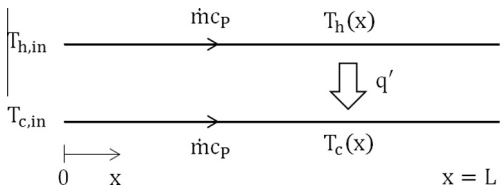

Fig. 4. Two parallel streams flowing in the same direction.

$$I_{\text{para}} = \int_0^1 \Delta T^2 d\xi = \frac{\Delta T_{\text{in}}^2}{2N}\left(1 - e^{-2N}\right) \tag{13}$$

When the two streams are arranged in counterflow, the local stream-to-stream temperature difference is independent of x. The counterflow analysis that replaces Eqs. (5) and (6) begins with

$$-\dot{m}c_P\, dT_h = q' dx \tag{14}$$

$$-\dot{m}c_P\, dT_c = q' dx \tag{15}$$

and, after using Eq. (7), shows that Eq. (8) is replaced by

$$\Delta T = \frac{\Delta T_{\text{in}}}{1+N} \tag{16}$$

The power density integral (13) is replaced by

$$I_{\text{counter}} = \frac{\Delta T_{\text{in}}^2}{(1+N)^2} \tag{17}$$

The relative merit of the parallel flow and the counterflow configurations is indicated by the ratio of Eqs. (13) and (17):

$$\frac{I_{\text{para}}}{I_{\text{counter}}} = \frac{(1+N)^2}{2N}\left(1 - e^{-2N}\right) \tag{18}$$

When $N \gg 1$, this ratio approaches a value much greater than 1,

$$\frac{I_{\text{para}}}{I_{\text{counter}}} \to \frac{N}{2} \gg 1 \tag{19}$$

When $N \ll 1$, Eq. (18) approaches 1. In between, for example at $N = 1$, Eq. (18) approaches 1.264, which indicates that the power density of the parallel flow configuration exceeds by 26.4% the power density of the counterflow configuration.

The conclusion that parallel flow is more advantageous than counterflow is important and fundamental. The fine channels with parallel flows are shown in Fig. 5. This finding is important because contrary to the first-designs shown in Figs. 1–3, the flow in the fine transversal flow channels should be oriented in parallel flow, not counterflow. It is fundamental because all the literature on the minimization of irreversibility (entropy generation, loss of available work) in heat exchangers demonstrates that counterflow is a better design than parallel flow (e.g. Ref. [1, p. 602]).

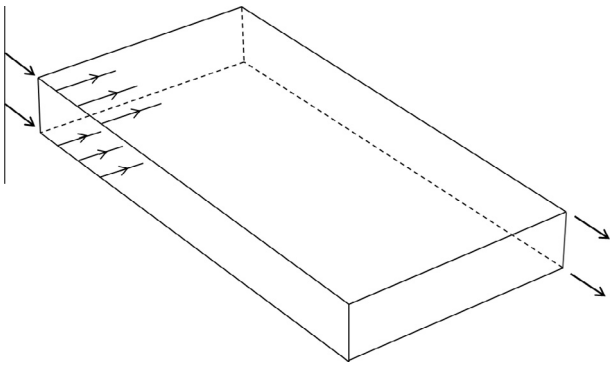

Fig. 5. Module with fine channels in parallel flow.

Why both conclusions are correct, parallel flow for the present TEM objective, and counterflow for power plant efficiency broadly Ref. [1, p. 602] is thermodynamics. Key in the present paper is that the parallel flow offers greater and greater power densities relative to counterflow as N increases, Eq. (19), that is as the fluid spends more time in residence in its channels, in longer and more tortuous channels. In this friction dominated limit, in addition to pursuing greater power density of generation it is important to pursue less and less pumping power for the fluid streams that bathe the two-flow structure of Fig. 4.

3. Mixed plenums

Another design alternative is to fit the hot end and cold end of the TEM with plenums in which the fluid is well mixed at T_H and T_L, respectively. In the hot plenum, the fluid temperature drops from $T_{h,in}$ to T_H, while in the cold plenum it rises from $T_{c,in}$ to T_L,

$$\dot{m}c_P\left(T_{h,in} - T_H\right) = UpL\left(T_H - T_L\right) \tag{20}$$

$$\dot{m}c_P\left(T_L - T_{c,in}\right) = UpL\left(T_H - T_L\right) \tag{21}$$

Adding Eqs. (20) and (21), we find that

$$\Delta T = \frac{\Delta T_{\text{in}}}{1+2N} \tag{22}$$

with the corresponding performance integral

$$I_{\text{mixed}} = \frac{\Delta T_{\text{in}}^2}{(1+2N)^2} \tag{23}$$

The above integral is smaller than the integral for counterflow,

$$\frac{I_{\text{counter}}}{I_{\text{mixed}}} = \frac{(1+2N)^2}{(1+N)^2} \tag{24}$$

This ratio tends to 4 as $N \gg 1$. In summary, the relative performance of the three designs is in favor of the parallel flow configuration, cf. Fig. 6,

$$I_{\text{para}} > I_{\text{counter}} > I_{\text{mixed}} \tag{25}$$

and the strength of the inequality signs increases monotonically as N increases. In the opposite limit, $N \ll 1$, the inequality signs are replaced by equal signs.

Friction is also a detrimental feature in the limit of fast flow where $N \ll 1$ and the two plates approach the isothermal description. This further enhances the importance of designing the flow architecture of each plate. We focus on this feature of the design in the next two sections.

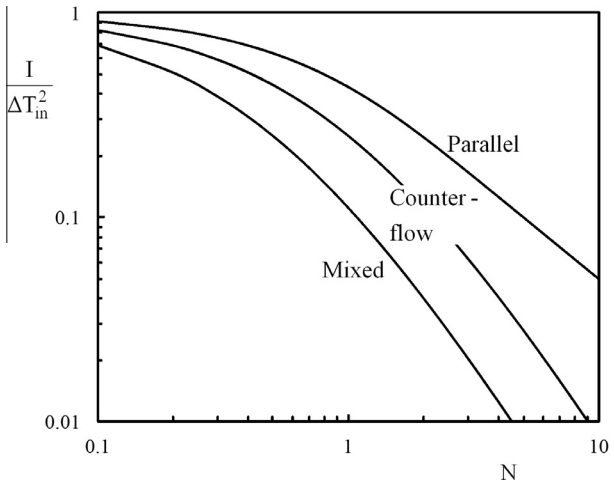

Fig. 6. The power performance of parallel flow, counter flow and mixed plenums.

4. Heat transfer and fluid friction losses

Consider next the broad view of the thermodynamic performance of the TEM. The uppermost level of performance is indicated in Eq. (4), which can be rewritten as

$$W_{\max} = \Delta T_{\text{in}}^2 \tilde{Z} \tag{26}$$

where $W_{\max}$ is the maximum power output $(I^2R)_{\max}$, $\Delta T_{\text{in}} = T_{\text{H}} - T_{\text{L}}$, and $\tilde{Z}$ is the Z-dependent function appearing on the right side of Eq. (4). The actual power output (W) is smaller than $W_{\max}$ because of two unavoidable design features: the temperature distribution on the two plates is not perfectly isothermal, and pumping power must be spent in order to push the hot and cold fluids through the vasculatures built into the plates.

Assume that the orientation of the two streams is in parallel flow, because according to the inequalities (25) the parallel flow design is superior to the other designs for any finite N. In the absence of pumping power losses, the actual power output W is equal to $I_{\text{para}}\,\tilde{Z}$, cf. Eqs. (4) and (13). When the pumping power $W_{\Delta P}$ is not negligible, the actual power output is

$$W = I_{\text{para}}\tilde{Z} - W_{\Delta P} \tag{27}$$

The lost power ($W_{\text{lost}} = W_{\max} - W$) is due to heat transfer and fluid friction effects combined,

$$W_{\text{lost}} = \Delta T_{\text{in}}^2 \tilde{Z} - I_{\text{para}}\tilde{Z} + W_{\Delta P} \tag{28}$$

which becomes

$$W_{\text{lost}} = W_{\Delta T} + W_{\Delta P} \tag{29}$$

where the $W_{\Delta T}$ term accounts for the loss due to the departure from temperature uniformity on the two plates,

$$W_{\Delta P} = \Delta T_{\text{in}}^2 \tilde{Z}\left(1 - \frac{1 - e^{-2N}}{2N}\right) \tag{30}$$

The dependence of $W_{\Delta T}$ on N is illustrated in Fig. 7: the heat transfer loss decreases monotonically as N decreases, and in the limit $N \ll 1$ it is represented by

$$W_{\Delta T} \cong \Delta T_{in}^2 \tilde{Z} N \tag{31}$$

The limit $N \ll 1$ means that the capacity rate $\dot{m}c_{\text{P}}$ is high enough to overtake $(k/t)A$ in the N definition (11), namely $N = \left(\frac{k}{t}\right)A/(\dot{m}c_{\text{P}})$ In this limit the flow rate $\dot{m}$ may be high enough so that the pumping power loss $W_{\Delta P}$ is not negligible relative to $W_{\Delta T}$.

The pump power is $W_{\Delta P} = 2\dot{m}\Delta P/(\rho\eta_p)$ where $\eta_p \leqslant 1$ is the pumping isentropic efficiency, assumed constant. The factor 2 means that there are two streams that must be pumped, i.e. two plates with channels.

Next, assume that the flow is fully developed and laminar in all the channels of the plate vasculature, and that the local ΔP losses are negligible. In this regime, the overall ΔP that must be maintained between the inlet and outlet of one plate obeys the form [20]

$$\Delta P = Cv\dot{m}\frac{L_s}{D_s^4} \tag{32}$$

where L_s and D_s^4 are the scales (dimensions) of the flow path length and channel diameters, and C is a dimensionless constant. In the next section we show that L_s, D_s and C depend on the configuration and size of the plate vasculature. At this point, we retain the conclusion that the overall pumping power increases monotonically with $\dot{m}^2$,

$$W_{\Delta P} = 2\frac{Cv}{\rho\eta_{\text{p}}}\frac{L_{\text{s}}}{D_{\text{s}}^4}\dot{m}^2 \tag{33}$$

Adding $W_{\Delta P}$ to the heat transfer loss in the small-N limit, Eq. (31), we obtain the total power loss expression

$$W_{\text{lost}} = \Delta T_{in}^2 \tilde{Z}\frac{(k/t)A}{\dot{m}c_{\text{P}}} + 2\frac{Cv}{\rho\eta_{\text{p}}}\frac{L_{\text{s}}}{D_{\text{s}}^4}\dot{m}^2 \tag{34}$$

which is of the form $W_{\text{lost}} = K_1\dot{m}^{-1} + K_2\dot{m}^2$. Fig. 8 shows that W_{lost} has a minimum, which is located at

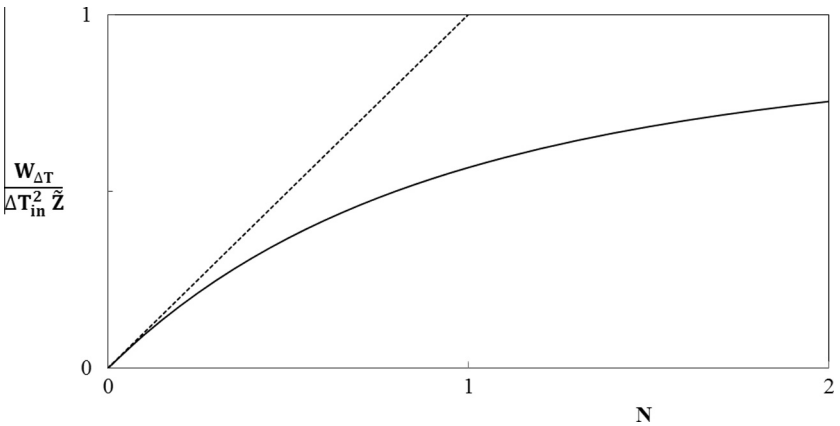

Fig. 7. The power loss $W_{\Delta T}$ decreases monotonically as N decreases.

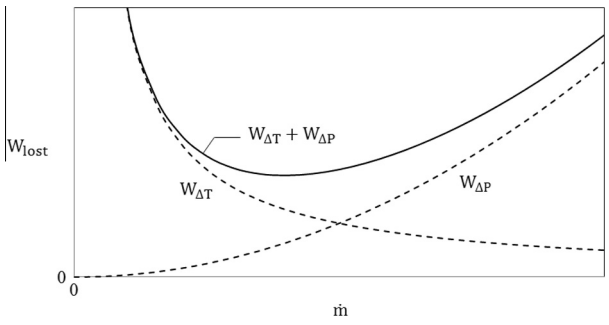

Fig. 8. The mass flow rate $\dot{m}$ resulting from the tradeoff between the ΔT and ΔP power losses.

$$\dot{m}_{opt} = \left(\frac{K_1}{2K_2}\right)^{1/3} \tag{35}$$

$$W_{lost,min} = \frac{3}{2^{2/3}} K_1^{2/3} K_2^{1/3} \tag{36}$$

with the notation

$$K_1 = \Delta T_{in}^2 \tilde{Z} \frac{kA}{c_p t} \tag{37}$$

$$K_2 = \frac{2Cv}{\rho \eta_p} \frac{L_s}{D_s^4} \tag{38}$$

Noteworthy is the effect of TEM geometry: K_1 is proportional to A/t, and K_2 is proportional to CL_s/D_s^4. This means that the minimum total loss of power is proportional to the geometric factor

$$G = \left(\frac{A}{t}\right)^{2/3} \left(\frac{CL_s}{D_s^4}\right)^{1/3} \tag{39}$$

Further reductions in $W_{lost,min}$ are possible by seeking flow architectures with smaller G values subject to the volumetric constraints that govern the TEM. This aspect of the constructal design exploration is detailed in the next section.

5. Vascular architecture

Consider the flow architecture embedded in one plate, Fig. 9, which consists of two trees matched canopy to canopy [20]. The first tree distributes the $\dot{m}$ stream to the plate area $A = HL$, and the second collects the stream from the area and guides it to the outlet. The trunk is a channel with transversal dimension D_1, and the n branches have the dimension D_2. Assume that n is large such that along the trunk the flow rate varies almost linearly between the opening (inlet, or outlet) and the closed end. In this case, the pressure drop along one of the D_1 trunks is

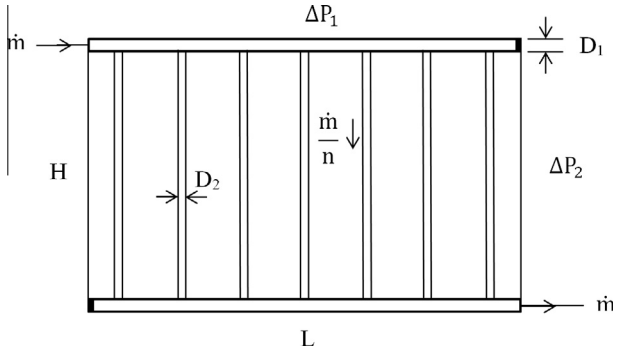

Fig. 9. Vascular design consisting of two trees matched canopy to canopy.

$$\Delta P_1 = Cv \frac{1}{2} \dot{m} \frac{L}{D_1^4} \tag{40}$$

where the factor $\frac{1}{2}$ is due to the linear variation of the mass flow rate, and C is the constant noted in Eq. (32), for example, $C = 128/\pi$ if the channel cross section is round.

Next, assume that the $\dot{m}$ stream is distributed almost uniformly to the n transversal branches. The applicability of this approximation is treated in detail in Ref. [22]. The pressure drop along one D_2 channel is

$$\Delta P_2 = Cv \frac{\dot{m}}{n} \frac{H}{D_2^4} \tag{41}$$

The overall pressure difference that drives the $\dot{m}$ stream is $\Delta P = \Delta P_1 + \Delta P_2$. The objective of the following analysis is to search for the flow configuration with the smallest flow resistance ($\Delta P/\dot{m}$) subject to the global finite-size constraints of the design. Combining Eqs. (40) and (41) leads to

$$\frac{\Delta P}{Cv\dot{m}} = \frac{L}{2D_1^4} + \frac{H}{nD_2^4} \tag{42}$$

which can vary subject to $A = HL$. The flow resistance is minimum when

$$\frac{H}{L} = \frac{n}{2} \left(\frac{D_2}{D_1}\right)^4 \tag{43}$$

$$L = \left(\frac{2A}{n}\right)^{1/2} \left(\frac{D_1}{D_2}\right)^2 \tag{44}$$

$$H = \left(\frac{nA}{2}\right)^{1/2} \left(\frac{D_2}{D_1}\right)^2 \tag{45}$$

$$\frac{\Delta P_{min}}{Cv\dot{m}} = \frac{(2A/n)^{1/2}}{(D_1 D_2)^2} \tag{46}$$

Further reductions in flow resistance can be achieved by maximizing the product D_1D_2. The two dimensions (D_1, D_2) are related through the requirement that the "printed area" of the vasculature must be a fraction (ϕ) of the plate area:

$$\phi = \frac{1}{A}(2D_1L + nD_2H) \tag{47}$$

By using Eqs. (44) and (45), the ϕ constraint becomes

$$\phi \frac{(2A)^{1/2}}{n^{3/2}} = \frac{4D_1^3}{n^2 D_2^2} + \frac{D_2^3}{D_1^2} \tag{48}$$

Minimizing the expression (46) subject to the constraint (48) we obtain

$$\frac{D_1}{D_2} = \left(\frac{n}{2}\right)^{2/5} \tag{49}$$

$$\frac{D_1}{A^{1/2}} = \phi n^{-3/10} 2^{-17/10} \tag{50}$$

$$\frac{D_2}{A^{1/2}} = \phi n^{-7/10} 2^{-13/10} \tag{51}$$

$$\left(\frac{\Delta P_{min}}{Cv\dot{m}}\right)_{min} = \frac{2^{13/2} n^{3/2}}{\phi^4 A^{3/2}} \tag{52}$$

Comparing the twice-minimized resistance (52) with the ΔP definition (32) that led to the G function (39), we conclude that the G value of the tree-tree design of Fig. 9 is

$$G = 2^{13/6} C^{1/3} \frac{n^{1/2} A^{1/6}}{\phi^{4/3} t^{2/3}} \tag{53}$$

In this geometric expression, the specified volume and design of the module dictate the values of A and t. For lower G values, the area

fraction ϕ should be larger, but ϕ cannot increase indefinitely because it must be smaller than 1. Finally, Eq. (53) suggests that a smaller n is better. This brings us to the question of how to select the spacing (L/n) between the D_2 channels. The answer is that the L/n spacing must be small enough (not greater than a threshold) such that the thermal resistance to lateral heat conduction along the solid plate (k_s), from the D_2 channel to the interstice, is not greater than the thermal resistance in the same direction through the fluid, from the $\dot{m}/n$ fluid to the internal surface of the D_2 channel:

$$\frac{L/n}{k_s D_2} < \frac{D_2}{k_f D_2} \tag{54}$$

In view of the results (44), (50) and (51), the inequality (54) becomes a lower bound for the projected tree–tree area fraction

$$\phi \geqslant 2\frac{k_f}{k_s} \tag{55}$$

If $\phi_c \sim k_f/k_s$ is the order of magnitude of this lower bound, and if $\phi \sim \phi_c$, the spacing δ between D_2 channels should have this order of magnitude:

$$\frac{\delta}{A^{1/2}} \sim n^{-7/10} \tag{56}$$

By using $n \sim L/\delta$ and Eqs. (44) and (49), we find that $\phi \sim \phi_c$ holds for any n value.

6. Illustrative example

As an illustration on how to configure the flow network, we start with the following assumptions:

- The dimensions of each plate are fixed ($L_p \times H_p$), together with the area on which the flow network is embedded ($L \times H$).
- The cross section of the channels is round. The channel diameter is D_1 and cannot exceed $D_{1,max}$.
- We learned from the constructal law that vascularization is a feature that allows us to decrease the overall pumping power of flow architectures. Therefore, channels with a diameter D_2 will be added, and their maximum value is also $D_{1,max}$.
- The total volume of fluid V_f is also fixed, which means that the plate porosity is fixed ($\varphi = V_f/V$, where V is the plate volume).
- The mass flow rate is also constrained.

Four configurations are studied: Configuration 1 corresponds to the sketch presented in Fig. 9. In this case, the channels of diameter D_1 serve for the distribution and the collection of the fluid. Their length L is greater than H, which is the length of the n tubes of diameter D_2. The spacing between the channels of diameter D_2 is d.

Configuration 2 (not presented here) is also a vascularized network but differs from configuration 1 in this respect: the distribution and collection channels of diameter D_1 are positioned on the H size of the domain, while the m parallel channels of diameter D_2 are placed in the L direction. These m channels are separated by a spacing t.

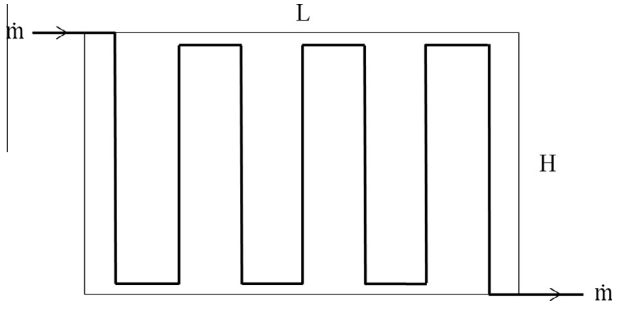

Fig. 10. Serpentine covering the entire plate area.

In Configuration 3, we replace the vascularized architecture by a single serpentine of diameter D_1. This configuration is sketched in Fig. 10. The spacing between the portions of the channel aligned with H remains at d.

Finally, Configuration 4 (not shown here) is the equivalent of configuration 3 but the meanders of the serpentine are placed along the L direction. In this way, the spacing between the portions of the channel aligned along L remains equal to t, as in Configuration 2. In sum, Configurations 3 and 4 offer the opportunity to compare the merit of a vascularized network in comparison with a linear occupation of the area.

Next, we evaluate the overall pressure losses in each configuration, assuming that the svelteness of the network defined as $Sv = (HL)^{1/2}/V_f^{1/3}$ is high enough so that the local pressure losses can be neglected. We obtain the following results:

Configuration 1

$$\Delta P = C\nu\dot{m}\left[\frac{d}{D_1^4}\sum_{k=1}^{n-1}\left(1-\frac{k}{n}\right)+\frac{H}{nD_2^4}\right] \tag{57}$$

For large n, we have $\sum_{k=1}^{n-1}(1-\frac{k}{n}) \cong \frac{n}{2}$, and

$$\Delta P = C\nu\dot{m}\left(\frac{n}{2}\frac{d}{D_1^4}+\frac{H}{nD_2^4}\right) \tag{58}$$

$$V_f = \frac{\pi}{4}(2D_1^2L + nD_2^2H) \tag{59}$$

$$L = d(n-1) \tag{60}$$

Configuration 2

$$\Delta P = C\nu\dot{m}\left(\frac{m}{2}\frac{t}{D_1^4}+\frac{L}{mD_2^4}\right) \tag{61}$$

$$V_f = \frac{\pi}{4}(2D_1^2H + mD_2^2L) \tag{62}$$

$$H = t(m-1) \tag{63}$$

Configuration 3

$$\Delta P = C\nu\dot{m}\frac{nH}{D_1^4} \tag{64}$$

$$V_f = \frac{\pi D_1^2}{4}nH \tag{65}$$

Configuration 4

$$\Delta P = C\nu\dot{m}\frac{mL}{D_1^4} \tag{66}$$

$$V_f = \frac{\pi D_1^2}{4}mL \tag{67}$$

Recall that the plate porosity φ is fixed. In Configurations 1 and 2, we are looking for the number of channels to implement (n in Configuration 1, m in configuration 2) and for the diameter ratio $r = D_1/D_2$ such that the overall pressure losses are minimum. Indeed, by minimizing the pressure losses with a fixed mass flow rate, means to minimize the pumping power.

We assume that the projected area of the flow network has the dimensions $L = 140$ mm and $H = 110$ mm. The plate porosity is $\varphi = 0.30$. Water at 20 °C flows at $\dot{m} = 9$ g/s through the channels which maximum diameter is $D_{1,max} = 2$ mm. The results corresponding to the first configuration are presented in Fig. 11. The overall pressure losses are minimum when the network is made of $n = 42$ channels of diameter D_2 connected to the distribution

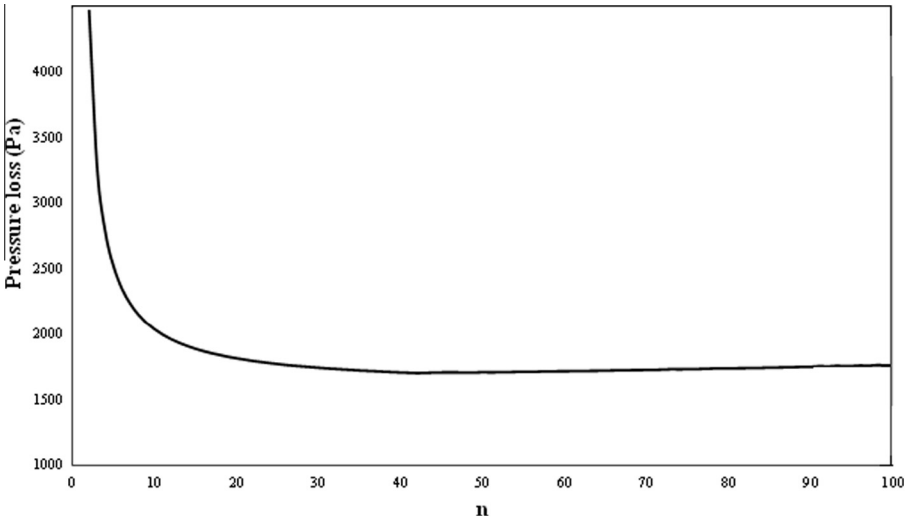

Fig. 11. Pressure losses as a function of the number of parallel channels, Configuration 1.

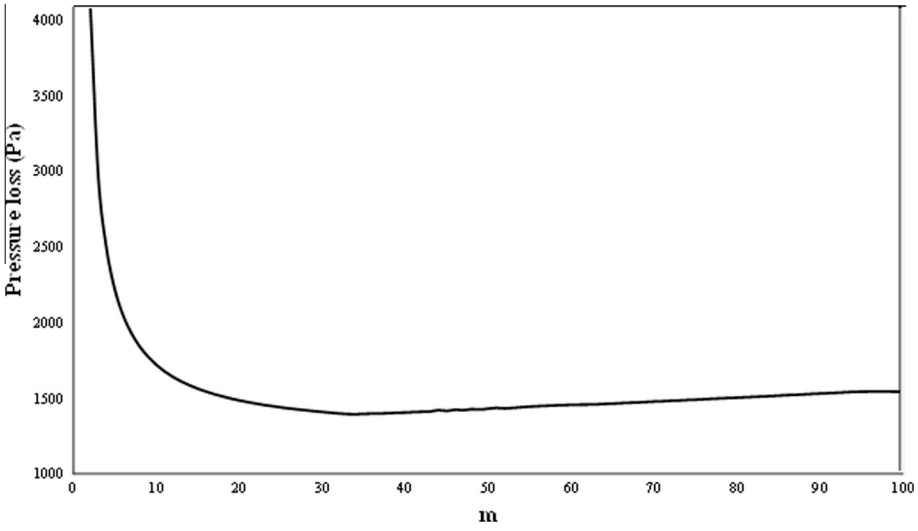

Fig. 12. Pressure losses as a function of the number of parallel channels, Configuration 2.

channel of diameter D_1 and to the collection channel of diameter D_1. This configuration corresponds to $D_1 = D_2 = 2$ mm, namely $r = 1$. We obtained $\Delta P = 1703$ Pa. Because the porosity is fixed, an increase in the number of channels corresponds to an increase in r and a decrease in the diameter D_2, which leads therefore to an increase in the pressure losses. Note that without constraining D_1 and D_2 to $D_{1,\max}$, the pressure losses would continuously increase with the number of channels in parallel.

Fig. 12 shows the evolution of the pressures losses in configuration 2. Again, a minimum can be reached when $m = 34$ channel in parallel. The diameter ratio is $r = 1.01$, the diameter D_1 is 2 mm, and the corresponding pressure losses are $\Delta P = 1396$ Pa. Note that in this configuration the number of channels in parallel is smaller, yet the channels are longer, compared to configuration 1.

Configuration 3, which is the serpentine analogous to the vascularized architecture of configuration 1 was analyzed in two ways. First we fixed the spacing d to be the same as the one obtained by optimizing configuration 1. In this case, because the porosity of the plate is fixed, the diameter D_1 should be of 2.92 mm, which is not acceptable because its maximum value should be 2 mm. Next, the diameter value is constrained to 2 mm. The corresponding spacing is $d = 1.59$ mm for a pressure drop of 225,017 Pa. In the case of configuration 4, an equivalent reasoning lead to $t = 3.23$ mm and $\Delta P = 1.113 \times 10^6$ Pa.

These results confirm the superiority of the constructal design: vascularization is the way to design the flow network.

7. Concluding remarks

The chief conclusions of this work are:

- The maximum power that can be obtained from a TEM system is proportional to the temperature difference squared.
- Counter-intuitively, parallel flows provide better performance (i.e. power density) than counter flows.
- Constructal theory allows to find the optimal geometric features for minimum pumping power and maximum power density
- Vascular architectures lead to better designs even when the maximum channels diameters are fixed provided the svelteness of the network is high enough.

Conflict of interest

None declared.

References

[1] A. Bejan, Advanced Engineering Thermodynamics, third ed., Wiley, Hoboken, 2006, pp. 675–680.
[2] A.Z. Sahin, B.S. Yilbas, The influence of operating and device parameters on the maximum efficiency and the maximum output power of thermoelectric generator, Int. J. Energy Res. 36 (2012) 111–119.
[3] A.Z. Sahin, B.S. Yilbas, The thermoelement as thermoelectric power generator: effect of leg geometry on the efficiency and power generation, Energy Convers. Manage. 65 (2013) 26–32.
[4] V.A. Semenyuk, Efficiency of cooling thermoelectric elements of arbitrary shape, J. Eng. Phys. Thermophys. 32 (1977) 196–200.
[5] K. Chen, S.B. Gwilliam, An analysis of the heat transfer rate and efficiency of TE (thermoelectric) cooling systems, Int. J. Energy Res. 20 (1996) 399–417.
[6] W.S. James, Optimal design of small ΔT thermoelectric generation systems, Energy Convers. Manage. 42 (2001) 709–720.
[7] L. Chen, J. Gong, F. Sun, C. Wu, Effect of heat transfer on the performance of thermoelectric generators, Int. J. Therm. Sci. 41 (2002) 95–99.
[8] S.B. Riffat, G.Q. Qiu, Design and characterization of a cylindrical, water-cooled heat sink for thermoelectric air-conditioners, Int. J. Energy Res. 30 (2006) 367–380.
[9] M. Gao, D.M. Rowe, Ring-structured thermoelectric module, Semicond. Sci. Technol. 22 (2007) 880–883.
[10] O. Yamashita, Effect of linear temperature dependence of thermoelectric properties on energy conversion efficiency, Energy Convers. Manage. 49 (2008) 3163–3169.
[11] R. Amatya, R.J. Ram, Solar thermoelectric generator for micropower applications, J. Electron. Mater. 39 (2010) 1735–1740.
[12] M. Freunek, M. Muller, T. Ungan, W. Walker, L.M. Reindl, New physical model for thermoelectric generators, J. Electron. Mater. 38 (2009) 1214–1220.
[13] R. Suzuki, D. Tanaka, Mathematical simulation of thermoelectric power generator with the multi-panels, J. Power Sources 122 (2003) 201–209.
[14] N. Vatcharasathien, J. Hirunlabh, J. Khedari, M. Daguenet, Design and analysis of solar thermoelectric power generation system, Int. J. Sustain. Energy 24 (2005) 115–127.
[15] X. Guo, H. Xiao, S. Yang, Modeling, experimental study and optimization on low-temperature waste heat thermoelectric generator system, Appl. Energy 87 (2010) 3131–3136.
[16] B.S. Yilbas, A.Z. Sahin, Thermoelectric device and optimum external load parameter and slenderness ratio, Energy 35 (2010) 5380–5384.
[17] O. Yamashita, Effect of linear and non-linear components in the temperature dependences of thermoelectric properties on the energy conversion efficiency, Energy Convers. Manage. 50 (2009) 1968–1975.
[18] M. Gillot, L. Jiang, S. Riffat, An investigation of thermoelectric cooling devices for small-scale space conditioning applications in buildings, Int. J. Energy Res. 34 (2010) 776–786.
[19] L. Chen, J. Li, F. Sun, C. Wu, Performance optimization for a two-stage thermoelectric heat pump with internal and external irreversibilities, Appl. Energy 85 (2008) 641–649.
[20] A. Bejan, S. Lorente, Design with Constructal Theory, Wiley, Hoboken, 2008.